**Chemistry–A European Journal**

Research Article
doi.org/10.1002/chem.202202206

**Chemistry Europe**
European Chemical
Societies Publishing

www.chemeurj.org

# Computational Insights of Selective Intramolecular O-atom Transfer Mediated by Bioinspired Copper Complexes

Stefani Gamboa-Ramirez,[a] Bruno Faure,[a] Marius Réglier,[a] A. Jalila Simaan,*[a] and Maylis Orio*[a]

**Abstract:** The stereoselective copper-mediated hydroxylation of intramolecular C–H bonds from tridentate ligands is reinvestigated using DFT calculations. The computational study aims at deciphering the mechanism of C–H hydroxylation obtained after reaction of Cu(I) precursors with dioxygen, using ligands bearing either activated (L$^1$) or non-activated (L$^2$) C–H bonds. Configurational analysis allows rationalization of the experimentally observed regio- and stereoselectivity. The computed mechanism involves the formation of a *side-on* peroxide species (**P**) in equilibrium with the key intermediate bis-(μ-oxo) isomer (**O**) responsible for the C–H activation step. The **P/O** equilibrium yields the same activation barrier for the two complexes. However, the main difference between the two model complexes is observed during the C–H activation step, where the complex bearing the non-activated C–H bonds yields a higher energy barrier, accounting for the experimental lack of reactivity of this complex under those conditions.

## Introduction

Oxidation reactions promoted by copper-containing enzymes are important for many vital biological processes.[1] These oxidation reactions are, in most cases, the result of dioxygen reductive activation at copper centers, leading to reactive Cu$_n$/O$_2$ species.[2–6] In particular, Cu-containing monooxygenases catalyzing the hydroxylation of C–H bonds under mild conditions and using dioxygen as co-oxidant have attracted attention.[7–11] Copper monooxygenases active sites are structurally diverse (nature of the ligands, nuclearity of the copper active sites, etc.), a diversity that allows for a modulation of their reactivity towards C–H bonds of different strengths from benzylic C–H bond of dopamine (Dopamine β Monooxygenase, DβM)[7] to the inert C–H bond of methane (particulate methane monooxygenase)[9,12] or polysaccharides (lytic polysaccharide monooxygenase).[13,14]

Over the last decades, bioinorganic chemists have prepared synthetic Cu complexes that mimic features of Cu-dependent monooxygenases in order to elucidate structure-function relationships and mechanistic pathways.[2–5,15] In particular, computational approaches combined with experimental data have provided valuable information on the structure and reactivity of copper-dioxygen (Cu$_n$/O$_2$) adducts, relevant to reactive species involved in C–H activation steps in enzymatic systems. Beyond fundamental aspects, the selective oxidation of organic molecules is of great importance for many industrial processes. Copper, an abundant metal with mild toxicity, is finding increasing applications in oxidative functionalization of molecules.[16–19] Therefore, understanding both the properties and the reactivity of diverse copper–oxygen adducts remains of great interest due to their potential in developing copper catalysts that can oxidatively activate strong C–H bonds.

Among the approaches developed by bioinorganic chemists, the so-called "substrate-ligand binding approach" consists in introducing a substrate on the ligand scaffold so that, if a reactive Cu$_n$/O$_2$ species is formed, it preferentially reacts with the internal substrate. This strategy was first reported by the groups of Karlin,[20] Réglier,[21–24] and Itoh.[25,26] Internal ligand oxidation has also been used by other groups to achieve the selective and preparative hydroxylation of aromatic or aliphatic C–H bonds.[17,27–35] Mechanistic studies have been conducted and it was recently proposed that, with bidentate imine-pyridine ligands, strong sp$^3$ C–H bond activation requires the formation of mononuclear Cu/O$_2$ species.[34,36] However, it is well established that the reaction conditions and the nature of the ligand (functions, denticity, size of chelate ring, etc.) strongly influence the formation and reactivity of copper-based systems.[32,36] Therefore, in the context of this work, we intend to use computational approaches to rationalize the reactivity of dinuclear Cu$_2$/O$_2$ species based on tridentate ligands.

[a] S. Gamboa-Ramirez, Dr. B. Faure, Dr. M. Réglier, Dr. A. J. Simaan, Dr. M. Orio
Aix Marseille Univ, CNRS
Centrale Marseille, iSm2, UMR 7313
52 Av. Escadrille Normandie Niemen,
13013 Marseille, (France)
E-mail: jalila.simaan@univ-amu.fr
maylis.orio@univ-amu.fr

**Chemistry–A European Journal**

Research Article
doi.org/10.1002/chem.202202206

**Chemistry Europe**
European Chemical
Societies Publishing

A few years ago, the group of Réglier designed tridentate RPy$_2$-type ligands (RPy$_2$ = (N,N-bis-[2-2(-pyridyl)ethyl] alkylamine)) bearing either an activated (IndanylPy$_2$ = IndPy$_2$; **L$^1$**) or non-activated (cyclopentylPy$_2$ = cPtPy$_2$; **L$^2$**) substrate. Starting from mononuclear Cu$^I$ complexes (**1-L$^1$** and **1-L$^2$**) in CH$_2$Cl$_2$, different results were obtained upon exposure to dioxygen (Scheme 1a).[22,23] Reaction with the activated ligand **L$^1$** yielded the stereoselectively hydroxylated *cis*-2-amino-1-indol product in 50% yield. When the non-activated **L$^2$** was used under the same reaction conditions, no hydroxylation was observed resulting in quantitative recovery of the initial ligand. In the case of RPy$_2$ type ligands, the reaction of Cu$^I$ with dioxygen has been shown to yield the dinuclear *side-on* peroxide species Cu$_2^{II}$(μ-η$^2$:η$^2$-O$_2$), denoted **P**, which is in equilibrium with the bis-(μ-oxo) isomer Cu$_2^{III}$(μ-O)$_2$, denoted **O** (Scheme 1b).[25,26,37–39] This oxo intermediate has been proposed to be responsible for the C–H abstraction step.[25,26] In the present paper, we investigated the ability of such dinuclear intermediates to perform C–H bond activation of **L$^1$** and **L$^2$** using a computational approach.

## Results and Discussion

Computational approaches have been previously used to study mononuclear[34] and dinuclear[31,40–42] Cu$_n$/O$_2$ adducts and their reactivity toward internal and external ligands. A detailed quantum chemistry investigation was conducted for **L$^1$** and **L$^2$** ligands to disclose the ability of the proposed {Cu$_2$O$_2$} intermediates 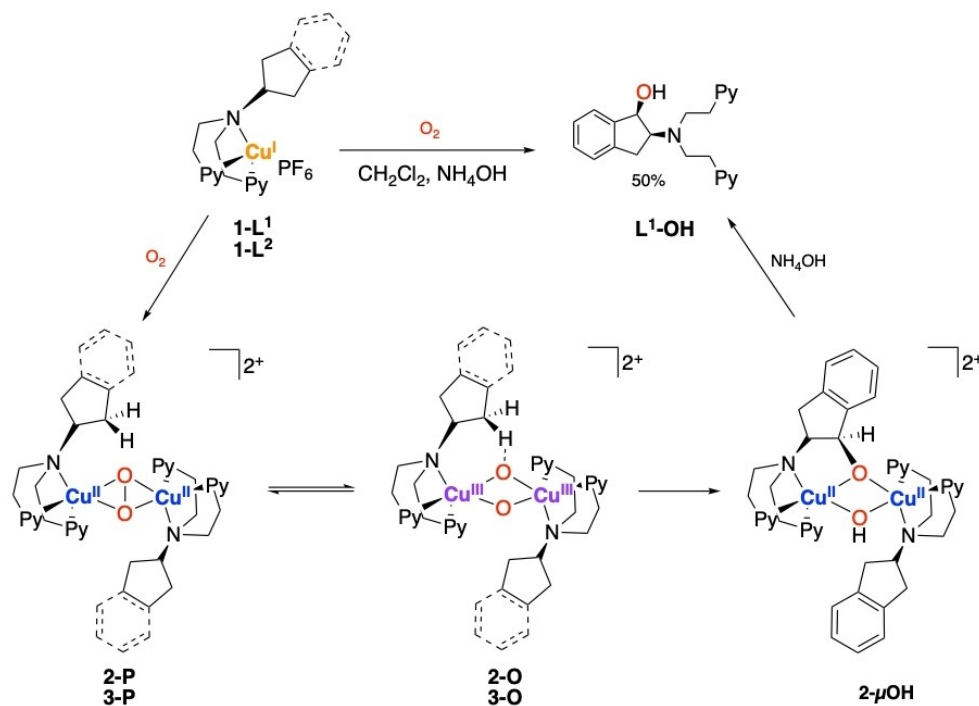to perform hydroxylation of C–H bonds. In addition, the experimental stereo- and regioselectivity of the reaction was also rationalized. A possible mechanism for **L$^1$** hydroxylation, derived from literature studies, is displayed on Scheme 2. Reaction of Cu(I) precursor with dioxygen leads to the formation of the peroxide species **2-P** when utilizing **L$^1$** (or **3-P** for **L$^2$**). The next step is the isomerization of **P** into the oxo species **2-O** (or **3-O** for **L$^2$**) which are reported as responsible for C–H activation steps.[25,26] In the case of **L$^1$**, the reaction yields the binuclear complex **2-μOH** and treatment with ammonium hydroxide (NH$_4$OH) leads to the release of the hydroxylated ligand (**L$^1$-OH**) with 50% yield. On the contrary, no hydroxylation is observed with **L$^2$**. Different mechanistic steps were confronted with the experimental observations to derive a structure property relationship between the ligand effect and the reactivity. Note that only one of the two copper-coordinating ligands gets hydroxylated upon reaction with dioxygen. Therefore, to construct and optimize the binuclear species, we considered model complexes holding one full ligand (**L$^1$** or **L$^2$**) on one copper center together with one truncated ligand **L$^3$** on the other one (Scheme S1).

### Ligand C–H bond-dissociation

Ligands **L$^1$** and **L$^2$** display internal substrates that are qualified as "activated" or "non-activated". To distinguish between them, bond dissociation energies (BDE) were evaluated for the different oxidizable positions of the ligands using free energy calculations and an implicit solvation model.[43] Three different
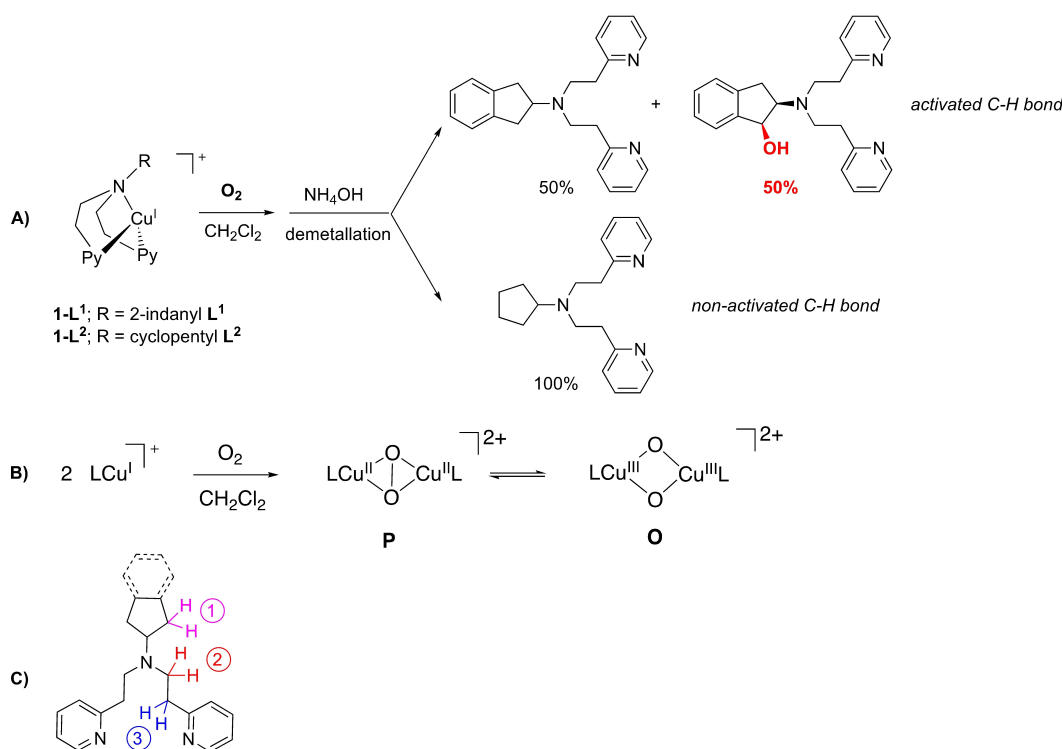


**Scheme 1.** A) Schematic representation of reaction of Cu$^I$ complexes with dioxygen and products formed using **L$^1$** and **L$^2$** ligands. B) Dinuclear Cu$_2$/O$_2$ species identified with RPy2-type ligands **C**) different oxidizable positions on the ligands.

Chemistry–A European Journal

Research Article
doi.org/10.1002/chem.202202206

Chemistry
Europe
European Chemical
Societies Publishing

**Scheme 2.** Schematic representation of the possible intermediate species in the hydroxylation reaction of $L^1$ and $L^2$ starting from mononuclear $1$-$L^1$ and $1$-$L^2$, respectively. Note that hydroxylation is not observed experimentally in the case of $L^2$.

positions were identified (Scheme 1C and Scheme S2): (1) the hydrogens on the substrate moiety, (2) the hydrogens in $\alpha$ position with respect to the central nitrogen and (3) the hydrogen in $\alpha$ position with respect to the pyridines. The BDE were calculated using the isolated ligands placed in dichloromethane, and results are displayed in Table 1. As expected, the BDE values for hydrogens in positions 2 and 3 are not significantly modified when comparing the two ligands. On the contrary, introduction of an aromatic ring (2-indanyl vs. cyclopentyl) leads to a decrease of the BDE at position 1 from 88.7 kcal mol$^{-1}$ in $L^2$ to 80.0 kcal mol$^{-1}$ in $L^1$. In the case of $L^1$, the difference in energy between the three positions is not very important since all BDEs are found to be around 80 kcal mol$^{-1}$, highlighting the fact that the observed regioselectivity (only position 1 oxidized) cannot be solely explained by this descriptor.

## Peroxo-oxo isomerism

The computational investigation of dinuclear copper species represents a major challenge due to the intrinsic nature of the dinuclear $Cu_2/O_2$ adducts. While the $Cu_2^{III}(\mu$-oxo) core (**O**)

**Table 1.** Bond Dissociation Energies (BDE, kcal mol$^{-1}$) for the different positions of ligands $L^1$ and $L^2$ in $CH_2Cl_2$.

| Ligand | Position 1 | Position 2 | Position 3 |
|--------|-----------|-----------|-----------|
| $L^1$ | 80.5 | 81.0 | 80.7 |
| $L^2$ | 88.7 | 79.8 | 80.0 |

displays two formal Cu(III) ions bound to two bridging $O^{2-}$ anions, the $Cu_2^{II}(\mu$-$\eta^2$:$\eta^2$-peroxo) isomer (**P**) features two Cu(II) ions coordinated to a $O_2^{2-}$ ligand. The **O** intermediate is formally a closed-shell system, and the **P** isomer is in an open-shell arrangement. Therefore, the isomerization equilibrium between **P** and **O** represents a bottleneck for computational methods since the singlet ground spin state cannot be properly described by a single determinant-methods, while multiconfigurational methods remain rather costly for medium-to-big sized systems.[44–48] Several groups recently reported that the **P**/**O** isomerism, featuring a very strong antiferromagnetic coupling for the **P** species, can be fairly described with a close-shell determinant.[44,46,49–53] The exchange coupling constant $J$ for complex **2-P** was calculated resulting in a very strong antiferromagnetic interaction between the two copper ions (see Supporting Information for details, Figures S2 and S3). Based on this finding, we envision the first mechanistic step as the cleavage of the O−O bond in the **P** complex leading to the formation of the **O** species. Relaxed surface scans were performed starting from complexes **2-P** and **3-P** using the O−O distance as reaction coordinate (Figures S4 and S5). Results show a small energy difference between the two oxo intermediates **2-O** and **3-O** (isomers **2-O**$_{ax\text{-}cis}$ and **3-O**$_{ax\text{-}cis}$, see below) with an activation barrier of $\Delta G^{\ddagger} = 8.4$ and 8.6 kcal mol$^{-1}$ via **TS$_{2\text{-}P/O}$** and **TS$_{3\text{-}P/O}$**, respectively (Figures 1, S1 and S5). The refined transition states feature an O−O distance of 1.781 Å and 1.798 Å (Figure S7) and display one single negative vibrational frequency at 310 and 300 cm$^{-1}$ assigned to the breathing mode of the O−O bonds found in the **2-P** and **3-P** complexes, respectively. It is worth noting that similar results were obtained

*Chem. Eur. J.* **2022**, *28*, e202202206 (3 of 7)

© 2022 The Authors. Chemistry - A European Journal published by Wiley-VCH GmbH

**Chemistry–A European Journal**

Research Article
doi.org/10.1002/chem.202202206

**Chemistry Europe**
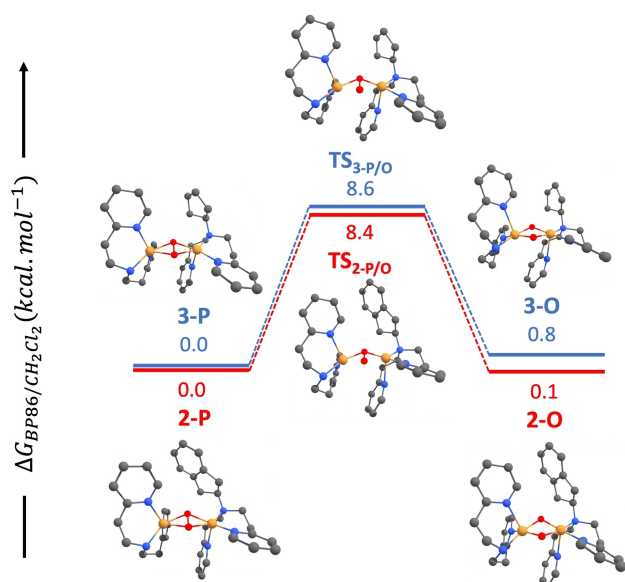European Chemical
Societies Publishing

**Figure 1.** Computed reaction pathway of the peroxo-oxo isomerization involving the **2-P** (red path) and **3-P** (blue path) complexes. Free energies are reported in kcal.mol$^{-1}$ and complexes **2-P** and **3-P** are used as reference for their corresponding pathway, i.e., 2-indanyl or cyclopentyl. Hydrogen atoms were removed for clarity.



**Figure 2.** Possible isomers of **2-O** with **L$^1$** ligand and their relative stabilities. Free energies are reported in kcal mol$^{-1}$ and hydrogen atoms were removed for clarity, except for hydrogen involved in the C–H activation.

from calculations using the Nudged Elastic Band[54] method (Figures S8 and S9). These results show that the oxo isomer, suggested to be the reactant for the C–H abstraction step, is thermodynamically accessible in both cases. In addition, they highlight that the two complexes, while having different overall reactivity, display a similar behavior for the isomerization reaction. Thus, these findings suggest the limited influence of the ligand on the peroxo-oxo isomerization.

## Regio- and stereo-selectivity

In principle, the oxo species formed during the hydroxylation reaction can adopt different conformations in which the substituent moiety could be placed either in the axial or facial position with respect to the copper centers. Additionally, the ligands **L$^1$** and **L$^2$** feature two pro-chiral hydrogen atoms which can potentially give rise to the *trans* or *cis* hydroxylation products. Three different models were constructed to assess the most stable conformer in the case of **L$^1$** (Figure 2): (1) substrate in the axial position with *cis* hydrogen facing the oxo bridge (axial-*cis*, **2-O$_{ax-cis}$**) (2) substrate in the axial position with *trans* hydrogen facing the oxo bridge (axial-*trans*, **2-O$_{ax-trans}$**), and (3) substrate in the facial position (facial, **2-O$_{fac}$**). Results indicate that the *cis* conformer with the *cis* hydrogen aligned to the Cu/O core in **2-O$_{ax-cis}$** is 9.8 and 8.9 kcal mol$^{-1}$ more stable than the *trans* and fac isomers (**2-O$_{ax-trans}$** and **2-O$_{fac}$**), respectively.

These data are thus supporting the observed stereoselectivity of the reaction as only the hydroxylated *cis*-2-amino-1-indol product was obtained.[22,23] When conducting such calculations for the **O** intermediate obtained with **L$^2$** (**3-O**), we reached
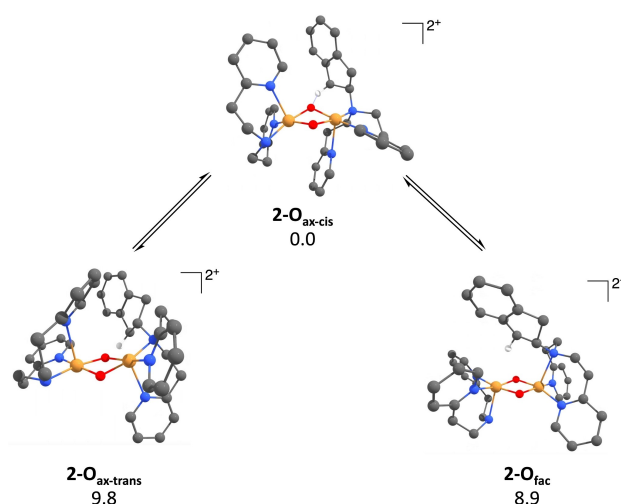
similar conclusions as for complex **2-O** (Figures S10). Indeed, the axial-*cis* position (**3-O$_{ax-cis}$**) is 6.6 kcal mol$^{-1}$ more stable than the facial position (**3-O$_{fac}$**), and 4.7 kcal mol$^{-1}$ more stable than the axial-*trans* conformation (**3-O$_{ax-trans}$**). Based on these findings and combining the results of the NBO analysis (Figures S11–S16 and Table S1), we restricted our computational study utilizing only the conformations having the substrate moieties in the axial-*cis* positions, i.e., **2-O$_{ax-cis}$** and **3-O$_{ax-cis}$**.

Finally, the regioselectivity of the experimentally observed oxidation in the case of **L$^1$** can also be explained by scrutinizing the favored isomer **2-O$_{ax-cis}$**. In the optimized structures of **2-O$_{ax-cis}$**, one can see that the hydrogen in position 2 is not located close to the Cu$_2$(μ-O)$_2$ core preventing from any intramolecular hydrogen abstraction at this position (Figure S6). In addition, the hydrogen in position 1 was found to be closer to the Cu$_2$(μ-O)$_2$ core than the one in position 3 (1.934 vs. 2.209 Å) (Figure S6). The optimized structure of **2-O$_{ax-cis}$** therefore accounts both for the experimentally observed regio- and stereo-selectivity of the intramolecular hydroxylation reaction. These findings are further supported by NBO analysis (see Supporting Information for details).

## Hydroxylation reaction

To further corroborate the above conclusions, we then considered the next step of the overall reaction: the C–H activation step. We performed relaxed surface scans, starting from complexes **2-O** and **3-O**, and using the O–H distance as reaction coordinate (Figures S19 and S20). Activation of the C–H bond of **2-O** via **TS$_{2-O/2-OH}$** into complex **2-OH** is associated with an activation barrier of $\Delta G^{\ddagger} = 1.9$ kcal mol$^{-1}$ with respect to the oxo species (Figure 3 and Figure S1). The optimized transition state features a hydrogen-carbon distance of 1.376 Å and a single negative vibrational frequency of 610 cm$^{-1}$ correspond-
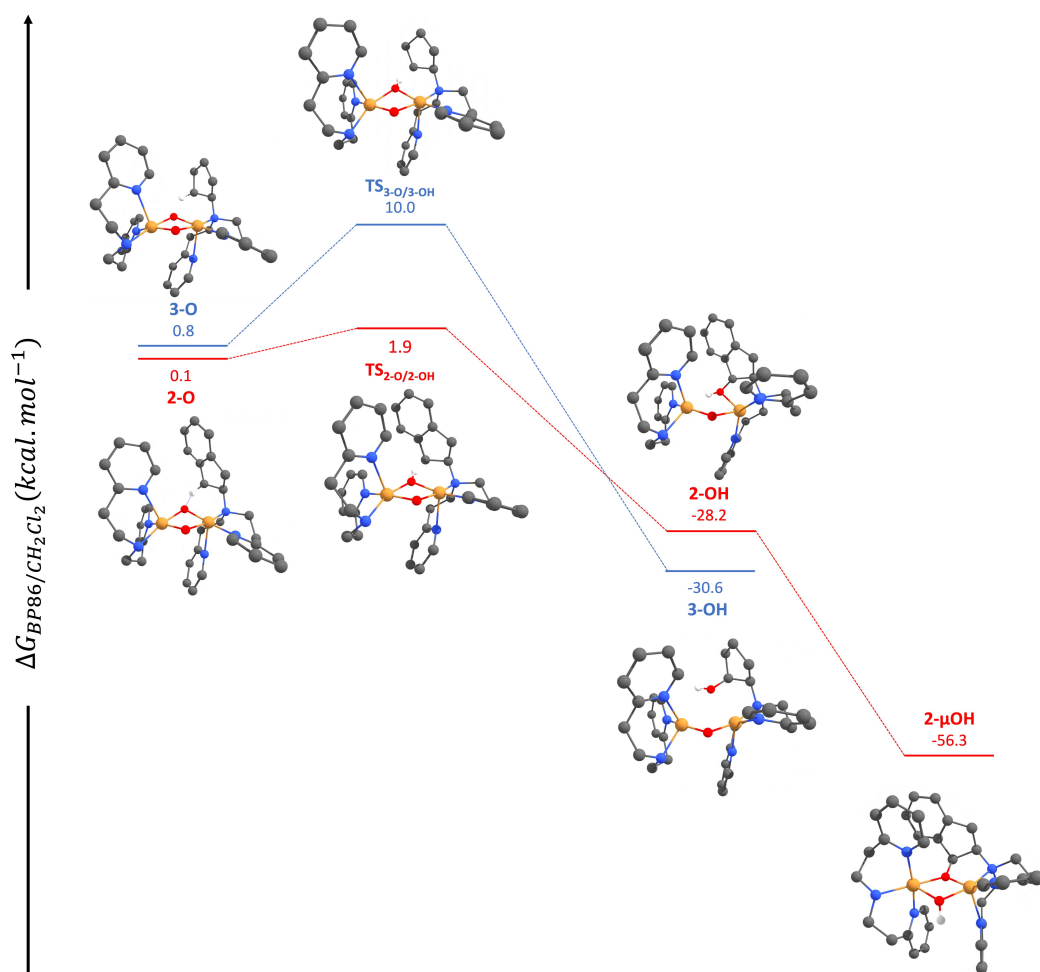
**Chemistry–A European Journal**

Research Article
doi.org/10.1002/chem.202202206

**Chemistry Europe**
European Chemical
Societies Publishing

**Figure 3.** Computed reaction pathway of the hydroxylation reaction involving the **2-O** (red path) and **3-O** (blue path) complexes. Free energies are reported in kcal mol$^{-1}$ and complexes **2-O** and **3-O** are used as reference. Hydrogen atoms were removed for clarity except the one involved in the reactivity.

ing to the hydrogen abstraction from the 2-indanyl moiety towards the oxygen of the oxo bridging ligand of the complex (Figure S21). Furthermore, formation of intermediate **2-OH** is strongly exergonic, featuring a reaction free energy $\Delta G_0 = -28.1$ kcal mol$^{-1}$ with respect to the oxo complex **2-O** (Figure 3). After hydroxylation, another step was described in the literature involving a proton transfer and the subsequent coordination of the hydroxylated moiety to form **2-μOH**, a dinuclear copper(II) (μ-oxo)(μ-hydroxo) complex.[25,26] Once again, this step is found to be highly exergonic with a reaction free energy $\Delta G_0 = -56.3$ kcal mol$^{-1}$ with respect to complex **2-O** (Figure 3).

Interestingly, when looking at the overall computed mechanism for the **L$^1$**-based model (Figure S1), it can be observed that the H-abstraction step has a rather low activation barrier as compared to the **P/O** isomerization step (1.9 vs. 8.4 kcal mol$^{-1}$, respectively). This suggests that **P/O** isomerization accounts for the rate determining step (r.d.s) of the reaction. These findings are in agreement with conclusions driven from kinetic studies by the group of Itoh with similar ligand systems.[25,26]

A much larger activation barrier of $\Delta G^{\pm} = 10.0$ kcal mol$^{-1}$ was computed for the C—H-abstraction by the oxo species **3-O** via **TS$_{3\text{-}O/3\text{-}OH}$** into complex **3-OH**. The optimized transition state features a hydrogen-carbon distance of 1.546 Å and a single negative vibrational frequency of 405 cm$^{-1}$ corresponding to the hydrogen abstraction from the cyclopentyl moiety towards the oxygen of the oxo bridge of the complex **3-OH** (Figure S21). Moreover, it is worth noting that the resulting hydroxylated moiety of complex **3-OH** does not coordinate the copper metal centers as for the case of **L$^1$**-based complex **2-O**. Finally, we want to emphasize that all above results are consistent with those obtained from calculations using the Nudged Elastic Band[54] method (Figures S22 and S23). These results are further supported by NBO analysis showing the existence of several stabilizing interactions between the indanyl and pyridine moieties of **L$^1$** (Figures S24–S26). Indeed, in the structure of complex **2-O**, two hydrogen atoms from a pyridine ligand on the other copper are found at distances of 2.767 and 3.472 Å from the indanyl centroid, respectively (Figure S26). Therefore, one can assume that the T-shaped edge-to-face conformation of the aromatic rings present in complex **2-O** will lead to

**Chemistry–A European Journal**

Research Article
doi.org/10.1002/chem.202202206

**Chemistry
Europe**
European Chemical
Societies Publishing

additional interactions that are not operative in **3-O**.[55] These non-covalent interactions possibly act as one of the driving forces during the hydroxylation step leading to a smaller relative barrier for H-abstraction in **2-O** when compared to **3-O**.

Our findings are thus consistent with the difference in reactivity observed when using ligand **L$^1$** and **L$^2$**, respectively, and provide a solid basis to rationalize the previous experimental observations.

## Conclusion

Hydroxylation of strong C–H bonds remains a challenging reaction. Using substrate-binding ligand approaches, several groups have observed non-activated C–H bond hydroxylation starting from Cu(I) or Cu(II) complexes placed in the presence of dioxygen or hydrogen peroxide.[17] In the case of bidentate ligands, it has been suggested that the reaction proceeds through the formation of mononuclear Cu(II)OOH entities, probably precursors of more oxidizing copper intermediates.[34–36] With ligands of higher denticity, dinuclear {Cu$_2$O$_2$} cores are proposed to be formed.

In the present work, we report a detailed computational mechanistic study of copper-mediated stereoselective intramolecular hydroxylation of C–H bond of tridentate RPy$_2$-type ligands.[22,23] To the best of our knowledge, the computational mechanistic study of **O**-type intermediates reactivity for intramolecular hydroxylation with tridentate ligands has not been addressed before. The present study provides a rationale for the experimental observations, addressing the regio- and stereoselectivity of benzylic C–H bond hydroxylation (**L$^1$**), and the lack of strong C–H bond activation of cyclopentyl substituent (**L$^2$**). We have computationally investigated the dinuclear *side-on* peroxide species (**P**) Cu$_2^{II}$(μ-η$^2$:η$^2$-O$_2$) and the key intermediate bis-(μ-oxo) isomer (**O**) Cu$_2^{III}$(μ-O)$_2$ that is proposed to be responsible for the C–H activation step.[25,26] In the case of indanyl-containing ligand (**L$^1$**), the **P/O** isomerization is found to be the r.d.s followed by a low-energy barrier H-abstraction step by the subsequently formed **O** intermediate. We found that the **P/O** isomerization is not significantly affected by the nature of the substrate on the ligand. However, the H-abstraction step from the cyclopentyl substituent (**L$^2$**) requires a significant activation energy as compared to the 2-indanyl one (**L$^1$**) explaining the absence of hydroxylation as it was reported experimentally. Our results therefore provide an explanation for low reactivity of **O** species based on tridentate RPy$_2$ ligands for strong C–H bond activation.

Interestingly, when Cu(II) precursors were placed in the presence of reducing agent (benzoin) and dioxygen, non-activated C–H bond hydroxylation was achieved.[22,23] This raises the question of the nature of the intermediates formed under these conditions. Further work is currently in progress to address this question.

## Experimental Section

All calculations were based on the Density Functional Theory (DFT) and were performed using the ORCA 4.2 program package.[56] Full geometry optimizations were carried out for all complexes in the high-spin state using the pure GGA functional BP86[57–59] in combination with the def2-TZVP[60,61] basis sets for all atoms. Dispersion correction was applied according to the method developed by Grimmer with the Becke-Johnson damping scheme (D3BJ).[62,63] Computational times were reduced by taking advantage of the resolution of the identity (RI) approximation in the Split-RI–J variant[64] with the appropriate Coulomb fitting sets.[65] Increased integration grids (Grid4 in ORCA convention) and tight SCF convergence criteria were used. To agree with the experimental conditions, calculations were performed in dichloromethane solvent by invoking the Control of the Conductor-like Polarizable Continuum Model (CPCM).[43] To ensure that the resulting structures converged to a local minimum on the potential energy surface, frequency calculations were performed and resulted in only positive normal vibrations for geometry optimizations, and in a single significant negative normal vibration for transitions state calculations. Relaxed surface scans were performed for both peroxo-oxo isomerization and hydroxylation reactions using the BP86 functional[57–59] with the def2-TZVP basis sets[60,61] for all atoms. Nudged Elastic Band method[54] was performed to verify the connection between minima and transition state for both peroxo-oxo isomerization and hydroxylation reactions. Gibbs free energies were computed from the optimized structures as a sum of electronic energy, solvation, and thermal corrections to the free energy. Natural Bond Orbital (NBO) analysis[66] was performed using the BP86[57–59] functional with the def2-TZVP[60,61] basis sets using the Gaussian 09 program package.[67] All chemical structure images were generated using Chemcraft.[68]

## Conflict of Interest

The authors declare no conflict of interest.

## Data Availability Statement

The data that support the findings of this study are available in the supplementary material of this article.

[1] E. I. Solomon, D. E. Heppner, E. M. Johnston, J. W. Ginsbach, J. Cirera, M. Qayyum, M. T. Kieber-Emmons, C. H. Kjaergaard, R. G. Hadt, L. Tianan, *Chem. Rev.* **2014**, *114*, 3659–3853.

[2] D. A. Quist, D. E. Diaz, J. J. Liu, K. D. Karlin, *J. Biol. Inorg. Chem.* **2016**, *22*, 253–288.

[3] C. E. Elwell, N. L. Gagnon, B. D. Neisen, D. Dhar, A. D. Spaeth, G. M. Yee, W. B. Tolman, *Chem. Rev.* **2017**, *117*, 2059–2107.

[4] A. J. Simaan, A. L. Concia, A. Munzone, M. C. Kafentzi, *Bioinspired Chemistry* **2019**, 185–263.

[5] W. Keown, J. B. Gary, T. D. P. Stack, *J. Biol. Inorg. Chem.* **2016**, *22*, 289–305.

[6] N. Fujieda, K. Umakoshi, Y. Ochi, Y. Nishikawa, S. Yanagisawa, M. Kubo, G. Kurisu, S. Itoh, *Angew. Chem. Int. Ed.* **2020**, *59*, 13385–13390; *Angew. Chem.* **2020**, *132*, 13487–13492.

[7] J. P. Klinman, *J. Biol. Chem.* **2006**, *281*, 3013–3016.

[8] C. A. Ramsden, P. A. Riley, *Bioorg. Med. Chem.* **2014**, *22*, 2388–2395.

[9] M. O. Ross, F. MacMillan, J. Wang, A. Nisthal, T. J. Lawton, B. D. Olafson, S. L. Mayo, A. C. Rosenzweig, B. M. Hoffman, *Science* **2019**, *364*, 566–570.

[10] B. Bissaro, A. K. Røhr, G. Müller, P. Chylenski, M. Skaugen, Z. Forsberg, S. J. Horn, G. Vaaje-Kolstad, V. G. H. Eijsink, *Nat. Chem. Biol.* **2017**, *13*, 1123–1128.

[11] G. R. Hemsworth, E. M. Johnston, G. J. Davies, P. H. Walton, *Trends Biotechnol.* **2015**, *33*, 747–761.

[12] S. I. Chan, W.-H. Chang, S.-H. Huang, H.-H. Lin, S. S.-F. Yu, *J. Inorg. Biochem.* **2021**, *225*, 111602.

[13] Z. Forsberg, M. Sørlie, D. Petrović, G. Courtade, F. L. Aachmann, G. Vaaje-Kolstad, B. Bissaro, Å. K. Røhr, V. G. Eijsink, *Curr. Opin. Struct. Biol.* **2019**, *59*, 54–64.

[14] L. Ciano, G. J. Davies, W. B. Tolman, P. H. Walton, *Nature Catalysis* **2018**, *1*, 571–577.

[15] S. Itoh, *Acc. Chem. Res.* **2015**, *48*, 2066–2074.

[16] S. D. McCann, S. S. Stahl, *Acc. Chem. Res.* **2015**, *48*, 1756–1766.

[17] R. Trammell, K. Rajabimoghadam, I. Garcia-Bosch, *Chem. Rev.* **2019**, *119*, 2954–3031.

[18] A. Das, Y. Ren, C. Hessin, M. D.-E. Murr, *Beilstein J. Org. Chem.* **2020**, *16*, 858–870.

[19] S. E. Allen, R. R. Walvoord, R. Padilla-Salinas, M. C. Kozlowski, *Chem. Rev.* **2013**, *113*, 6234–6458.

[20] Z. Tyeklár, K. D. Karlin, *Acc. Chem. Res.* **1989**, *22*, 241–248.

[21] M. Réglier, E. Amadéi, R. Tadayoni, B. Waegell, *J. Chem. Soc. Chem. Commun.* **1989**, *8*, 447–450.

[22] I. Blain, M. Giorgi, I. D. Riggi, M. Réglier, *Eur. J. Inorg. Chem.* **2000**, 393–398.

[23] I. Blain, P. Bruno, M. Giorgi, E. Lojou, D. Lexa, M. Réglier, *Eur. J. Inorg. Chem.* **1998**, 1297–1304.

[24] M.-C. Kafentzi, R. Papadakis, F. Gennarini, A. Kochem, O. Iranzo, Y. L. Mest, N. L. Poul, T. Tron, B. Faure, A. J. Simaan, M. Réglier, *Chem. Eur. J.* **2018**, *24*, 5213–5224.

[25] S. Itoh, M. Taki, H. Nakao, P. L. Holland, W. B. Tolman, L. Que Jr., S. Fukuzumi, *Angew. Chem. Int. Ed.* **2000**, *39*, 398–400; *Angew. Chem.* **2000**, *112*, 409–411.

[26] S. Itoh, H. Nakao, L. M. Berreau, T. Kondo, M. Komatsu, S. Fukuzumi, *J. Am. Chem. Soc.* **1998**, *120*, 2890–2899.

[27] B. Schönecker, T. Zheldakova, C. Lange, W. Günther, H. Görls, M. Bohl, *Chem. Eur. J.* **2004**, *10*, 6029–6042.

[28] B. Schönecker, C. J. Lange, *Organomet. Chem.* **2006**, *691*, 2107–2124.

[29] B. Schönecker, T. Zheldakova, Y. Liu, M. Kötteritzsch, W. Günther, H. Görls, *Angew. Chem. Int. Ed.* **2003**, *42*, 3240–3244; *Angew. Chem.* **2003**, *115*, 3361–3365.

[30] J. Becker, P. Gupta, F. Angersbach, F. Tuczek, C. Näther, M. C. Holthausen, S. Schindler, *Chem. Eur. J.* **2015**, *21*, 11735–11744.

[31] J. Becker, Y. Y. Zhyadlo, E. D. Butova, A. A. Fokin, P. R. Schreiner, M. Förster, M. C. Holthausen, P. Specht, S. Schindler, *Chem. Eur. J.* **2018**, *24*, 15543–15549.

[32] A. Petrillo, A. Hoffmann, J. Becker, S. Herres-Pawlis, S. Schindler, *Eur. J. Inorg. Chem.* **2022**, DOI 10.1002/ejic.202100970.

[33] R. Trammell, Y. Y. See, A. T. Herrmann, N. Xie, D. E. Diaz, M. A. Siegler, P. S. Baran, I. Garcia-Bosch, *J. Org. Chem.* **2017**, *82*, 7887–7904.

[34] R. Trammell, L. D'Amore, A. Cordova, P. Polunin, N. Xie, M. A. Siegler, P. Belanzoni, M. Swart, I. Garcia-Bosch, *Inorg. Chem.* **2019**, *58*, 7584–7592.

[35] P. Specht, A. Petrillo, J. Becker, S. Schindler, *Eur. J. Inorg. Chem.* **2021**, 1961–1970.

[36] S. Zhang, R. Trammell, A. Cordova, M. A. Siegler, I. Garcia-Bosch, *J. Inorg. Biochem.* **2021**, *223*, 111557.

[37] I. Sanyal, M. Mahroof-Tahir, M. S. Nasir, P. Ghosh, B. I. Cohen, Y. Gultneh, R. W. Cruse, A. Farooq, K. D. Karlin, *Inorg. Chem.* **1992**, *31*, 4322–4332.

[38] E. Pidcock, S. DeBeer, H. V. Obias, B. Hedman, K. O. Hodgson, K. D. Karlin, E. I. Solomon, *J. Am. Chem. Soc.* **1999**, *121*, 1870–1878.

[39] H. V. Obias, Y. Lin, N. N. Murthy, E. Pidcock, E. I. Solomon, M. Ralle, N. J. Blackburn, Y.-M. Neuhold, A. D. Zuberbühler, K. D. Karlin, *J. Am. Chem. Soc.* **1998**, *120*, 12960–12961.

[40] P. Spuhler, M. C. Holthausen, *Angew. Chem. Int. Ed.* **2003**, *42*, 5961–5965; *Angew. Chem.* **2003**, *115*, 6143–6147.

[41] Y. F. Liu, J. G. Yu, P. E. M. Siegbahn, M. R. A. Blomberg, *Chem. Eur. J.* **2013**, *19*, 1942–1954.

[42] P. Gupta, M. Diefenbach, M. C. Holthausen, M. Förster, *Chem. Eur. J.* **2017**, *23*, 1427–1435.

[43] V. Barone, M. Cossi, *J. Phys. Chem. A* **1998**, *102*, 1995–2001.

[44] M. Flock, K. Pierloot, *J. Phys. Chem. A* **1999**, *103*, 95–102.

[45] M. F. Rode, H.–J. Werner, *Theor. Chem. Acc.* **2005**, *114*, 309–317.

[46] C. J. Cramer, M. Wloch, P. Piecuch, C. Puzzarini, L. Gagliardi, *J. Phys. Chem. A.* **2006**, *110*, 1991–2004.

[47] P. A. Malmqvist, K. Pierloot, A. R. M. Shahi, C. J. Cramer, L. Gagliardi, *J. Chem. Phys.* **2008**, *128*, 204109.

[48] M. Rohrmüller, A. Hoffmann, C. Thierfelder, S. Herres-Pawlis, W. G. Schmidt, *J. Compt. Chem.* **2015**, *36*, 1672–1685.

[49] A. Béceres, *Inorg. Chem.* **1997**, *36*, 4831–4837.

[50] B. F. Gherman, C. J. Cramer, *Coord. Chem. Rev.* **2009**, *253* 723–753.

[51] D. G. Liakos, F. Neese, *J. Chem. Theory Comput.* **2011**, *7*, 1511–1523.

[52] A. Hoffmann, S. Herres-Pawlis, *Chem. Commun.* **2014**, *50*, 403–405.

[53] A. Hoffmann, M. Wern, T. Hoppe, M. Witte, R. Haase, P. Liebhäuser, J. Glatthaar, S. Herres-Pawlis, S. Schindler, *Eur. J. Inorg. Chem.* **2016**, 4744–4751.

[54] V. Ásgeirsson, B. O. Birgisson, R. Bjornsson, U. Becker, F. Neese, C. Riplinger, H. Jónsson, *J. Chem. Theory Comput.* **2021**, *17*, 4929–4945.

[55] L. M. Salonen, M. Ellermann, F. Diederich, *Angew. Chem. Int. Ed.* **2011**, *50*, 4808–4842; *Angew. Chem.* **2011**, *123*, 4908–4944.

[56] F. Neese, *Wiley Interdiscip. Rev.: Comput. Mol. Sci.* **2012**, *2*, 73–78.

[57] J. P. Perdew, *Phys. Rev. B* **1986**, *33*, 8822–8824.

[58] J. P. Perdew, *Phys. Rev. B* **1986**, *34*, 7406.

[59] A. D. Becke, *Phys. Rev. A* **1988**, *38*, 3098–3100.

[60] A. Schäfer, C. Huber, R. J. Ahlrichs, *Chem. Phys.* **1994**, *100*, 5829–5835.

[61] F. Weigend, R. Ahlrichs, *Phys. Chem. Chem. Phys.* **2005**, *7*, 3297–3305.

[62] S. Grimme, J. Antony, S. Ehrlich, H. Krieg, *J. Chem. Phys.* **2010**, *132*, 154104.

[63] S. Grimme, S. Ehrlich, L. Goerigk, *J. Comput. Chem.* **2011**, *32*, 1456–1465.

[64] F. Neese, *J. Comput. Chem.* **2003**, *24*, 1740–1747.

[65] F. Weigend, *Phys. Chem. Chem. Phys.* **2006**, *8*, 1057–1065.

[66] NBO 6.0. E. D. Glendening, J. K. Badenhoop, A. E. Reed, J. E. Carpenter, J. A. Bohmann, C. M. Morales, C. R. Landis, and F. Weinhold, Theoretical Chemistry Institute, University of Wisconsin, Madison **2013**; http://nbo6. chem.wisc.edu/.

[67] M. J. Frisch, G. W. Trucks, H. B. Schlegel, G. E. Scuseria, M. A. Robb, J. R. Cheeseman, G. Scalmani, V. Barone, B. Mennucci, G. A. Petersson, H. Nakatsuji, M. Caricato, X. Li, H. P. Hratchian, A. F. Izmaylov, J. Bloino, G. Zheng, J. L. Sonnenberg, M. Hada, M. Ehara, K. Toyota, R. Fukuda, J. Hasegawa, M. Ishida, T. Nakajima, Y. Honda, O. Kitao, H. Nakai, T. Vreven, J. A. Montgomery, Jr., J. E. Peralta, F. Ogliaro, M. Bearpark, J. J. Heyd, E. Brothers, K. N. Kudin, V. N. Staroverov, T. Keith, R. Kobayashi, J. Normand, K. Raghavachari, A. Rendell, J. C. Burant, S. S. Iyengar, J. Tomasi, M. Cossi, N. Rega, J. M. Millam, M. Klene, J. E. Knox, J. B. Cross, V. Bakken, C. Adamo, J. Jaramillo, R. Gomperts, R. E. Stratmann, O. Yazyev, A. J. Austin, R. Cammi, C. Pomelli, J. W. Ochterski, R. L. Martin, K. Morokuma, V. G. Zakrzewski, G. A. Voth, P. Salvador, J. J. Dannenberg, S. Dapprich, A. D. Daniels, O. Farkas, J. B. Foresman, J. V. Ortiz, J. Cioslowski, D. J. Fox, *Gaussian 09, Revision D.01*, Gaussian, Inc., Wallingford CT, **2013**.

[68] Chemcraft, http://chemcraftprog.com.